Stopping of ions based on semiclassical phase shifts

N. R. Arista[1] and P. Sigmund[2]
[1]*División Colisiones Atómicas, Centro Atómico Bariloche and Instituto Balseiro, AR-8400 Bariloche, Argentina*
[2]*Department of Physics and Chemistry, University of Southern Denmark, DK-5230 Odense M, Denmark*
(Received 21 February 2007; revised manuscript received 19 October 2007; published 28 December 2007)

We develop a semiclassical theory of the stopping of ions in matter, aiming at a wide validity range in terms of ion energies and mass number. The excitation of a target electron is described as a binary ion-electron interaction governed by a screened-Coulomb potential. The energy loss is expressed in terms of the transport cross section for electron-ion scattering which is calculated in a semiclassical approximation to the scattering phase shifts. Exact numerical integrations of the Schrödinger equation are used for quantitative tests of the derived results. This approach provides a nonperturbative representation of the energy loss which bridges the gap between classical and quantal descriptions. It applies to nonrelativistic velocities for light and heavy ions with arbitrary charge states, and it reproduces typical quantum phenomena such as the oscillatory atomic-number dependence of stopping cross sections at low energies. Calculated results have been compared with predictions from linear and nonlinear stopping theory, in particular for stopping in the electron gas and by a quantum harmonic oscillator. Moreover, attention has been paid to the Bloch correction which, in the present scheme, approaches Bloch's well-known expression but does not blow up at low projectile speed. We have also determined a generalized Bloch correction which depends on the ion charge. Particular attention has been given to the description of static and dynamic screening of a dressed ion.

DOI: 10.1103/PhysRevA.76.062902 PACS number(s): 34.50.Bw

I. INTRODUCTION

The passage of charged particles through matter has been studied extensively over more than a hundred years. A favored object of study among theoreticians has been the understanding of the energy loss, or stopping of ions in matter [1–3]. This is a field developed to a high degree of detail and sophistication, but the cumulative theoretical effort has been spread rather unevenly over various regimes of interest:

(i) As regards projectiles, the dominating effort has been directed toward particles with low charge, in particular protons.

(ii) As regards stopping media, early theories [4–6] focused on the interaction with individual atoms, but attention gradually turned over to the free-electron gas. This enables accurate estimates of stopping parameters for conduction electrons in metals. Application to gases or insulating solids is less quantitative, dependent on the velocity regime.

(iii) As regards beam velocities, the high-speed regime has been most intensely studied. This refers to projectile speeds $v \gg Z_1 v_0$, where Z_1 is the atomic number of a projectile ion and v_0 the Bohr velocity. In the opposite limit of low projectile speed, $v < v_0$, significant progress has been achieved for light-ion stopping in the Fermi gas, thanks to the application of tools from condensed-matter physics [7]. However, there are wide regions in the ion-target-velocity parameter space that are not covered by either of these approaches.

Much has been learned during the past decade about stopping of swift heavy ions, as summarized in Refs. [8,9]. In addition to our own rather complementary approaches [10,11] we mention Refs. [12,13] as well as earlier work quoted in all four papers. Taken together, these tools serve as a fairly solid basis for estimating stopping parameters over a very broad range of ion-target combinations as well as beam velocities.

A fundamental weakness at the present stage is the lack of a unifying approach to stopping theory. The Born approximation is a powerful tool for low Z_1 and high v, but its range of validity is quite restricted, especially in the absence of higher-order terms and shell corrections. Conversely, Bohr's classical theory is a very useful starting point in the study of heavy-ion stopping, but to convert it into a quantitative tool requires incorporation of an impressive number of corrections. The Bloch correction provides a convenient link between the Bohr and the Bethe scheme, but it needs to be added as a separate entity in the above approaches.

The present paper reports an attempt to come closer to a unified theory, eliminating some, although not all, existing shortcomings. Our starting point is the assumption that the main stopping mechanism is excitation and ionization of target electrons via Coulomb scattering. Projectile excitation may be significant at medium to low projectile speed, but will be left out here. While the cross sections for free-Coulomb scattering in classical and nonrelativistic quantum mechanics are identical, the electron fluxes around the scattering center are not [14,15], and hence the scattering distributions after allowance for electron binding differ in classical and quantum mechanics. This is the origin of the Bloch correction and related effects.

According to the Bohr picture, the dominating effect of the binding of target electrons is the limitation of the free-Coulomb interaction to within an adiabatic radius. This limitation may be reinterpreted as a screening of the projectile-target interaction [16], a feature that has been utilized frequently in the past. The two schemes developed by the present authors [10,11,17,18] belong in this category, and the present work provides a link between them.

Differences between these treatments lie mostly in the way on how binary scattering theory is handled. Reference [11] is a quantum theory, while Ref. [17] operates with classical scattering theory, and quantum mechanics is superim-

posed via an inverse-Bloch correction. Conversely, the description of distant collisions is asymptotically exact in Ref. [17], but approximate in [11]. Further differences concern screening function and screening radius as well as the velocity spectra characterizing the orbital motion of target electrons. Both approaches contain the Z_1 asymmetry (Barkas-Andersen effect) from the beginning, and shell corrections as well as atomic screening due to projectile electrons are incorporated in a transparent manner.

The most significant feature in the present work is the use of semiclassical scattering theory for screened-Coulomb interaction, which is a compromise between the analytical simplicity and transparency of classical theory and the rigor of exact quantum scattering theory. The procedure makes use of WKB phase shifts. These phase shifts exist in a perturbative and a nonperturbative version [19,20]. While already the perturbative version generates a significant improvement compared to linear stopping theory, nonperturbative WKB phase shifts are found to be almost equivalent to exact phase shifts for the processes considered here. Using these tools we reformulate the theory of stopping of ions in matter in a rather comprehensive way, allowing for a wide range of possible applications.

II. GENERAL SCHEME

A. Preliminaries

A key quantity in stopping theory [3] is the stopping cross section S per target electron, which is conventionally written in the form

$$S = \frac{4\pi Z_1^2 e^4}{mv^2} L, \tag{1}$$

where the dimensionless stopping number L reflects the detailed physical model governing the stopping process.

For a binary collision with a target electron initially at rest, the stopping cross section $S^{(0)}$ can be expressed as

$$S^{(0)} = mv^2 \sigma_{\rm tr}, \tag{2}$$

where the transport cross section $\sigma_{\rm tr}$ is defined by

$$\sigma_{\rm tr} = \int (1 - \cos\,\theta) d\sigma(\theta), \tag{3}$$

and θ is the center-of-mass scattering angle. Expressed in terms of quantum-mechanical phase shifts δ_ℓ, $\sigma_{\rm tr}$ reads

$$\sigma_{\rm tr} = \frac{4\pi}{k^2} \sum_{\ell=0}^{\infty} (\ell + 1) \sin^2(\delta_\ell - \delta_{\ell+1}), \tag{4}$$

where $k = mv/\hbar$ is the electron wave number in the projectile reference frame.

Hence, the stopping number $L^{(0)}$ for electrons at rest is given by

$$L^{(0)} = \frac{1}{\eta^2} \sum_{\ell=0}^{\infty} (\ell + 1) \sin^2(\delta_\ell - \delta_{\ell+1}), \tag{5}$$

where

$$\eta = \frac{Z_1 e^2}{\hbar v} \tag{6}$$

is the Sommerfeld parameter. The quantity $\kappa = 2\eta$ is Bohr's kappa parameter which limits the "classical" from the Born regime.

Incorporation of the orbital motion of the target electron is achieved by a simple transformation which is to be discussed below.

B. Semiclassical approach

For a given ion-electron interaction potential $V(r)$, phase shifts can be evaluated rigorously by solving the Schrödinger equation

$$\frac{d^2 u_\ell}{dr^2} + \left(k^2 - \frac{\ell(\ell+1)}{r^2} - \frac{2m}{\hbar^2} V(r) \right) u_\ell(r) = 0 \tag{7}$$

for the radial wave function $u_l(r)$, which has the asymptotic form $u_\ell \sim \sin(kr - \ell\pi/2 + \delta_\ell)$ at large distances. Phase shifts δ_ℓ so obtained—henceforth to be called "exact"—will serve as a test to the approximations considered in the following.

Here we focus on the semiclassical or WKB approximation [19,20], according to which

$$\delta_\ell = \int dr \sqrt{k^2 - \frac{(\ell + 1/2)^2}{r^2} - \frac{2mV(r)}{\hbar^2}} - \int dr \sqrt{k^2 - \frac{(\ell + 1/2)^2}{r^2}}. \tag{8}$$

Integrations go over the intervals where the radicands are positive. Results found by means of phase shifts determined from Eq. (8) will be referred to in the following as SCL1.

A perturbative version of Eq. (8) is found by expansion up to first order in powers of the potential,

$$\delta_\ell^{\rm pert} \simeq -\frac{m}{\hbar^2} \int dr \frac{V(r)}{\sqrt{k^2 - (\ell + 1/2)^2/r^2}}. \tag{9}$$

C. Yukawa potential

The Yukawa potential

$$V(r) = -\frac{Z_1 e^2}{r} e^{-r/a} \tag{10}$$

has been found to be a useful model potential in the present context, in particular for swift ions where Bohr's adiabatic radius [1]

$$a_{\rm ad} = \frac{v}{\omega} \tag{11}$$

may be chosen [10,21] as the screening radius a. Here, ω is a characteristic resonance frequency of a target atom or, if the stopping medium is an electron gas, the plasma frequency.

1. Perturbative solution

The differential cross section in the Born approximation for scattering on a Yukawa potential is well known and reads [3]

$$d\sigma(\theta) = \left(\frac{b}{4}\right)^2 \frac{2\pi \sin\theta d\theta}{[\sin^2(\theta/2) + 1/B^2]^2}, \tag{12}$$

where $b=2Z_1e^2/mv^2$ is the classical collision diameter, $B=2a/\lambda\!\!\!^{-}$, and $\lambda\!\!\!^{-}=\hbar/mv$ the de Broglie wavelength.

Integration in accordance with Eq. (3) yields the stopping cross section

$$S^{(0)} = mv^2\sigma_{\rm tr} = \frac{2\pi Z_1^2 e^4}{mv^2}\left(\ln(1+B^2) - 1 + \frac{1}{1+B^2}\right). \tag{13}$$

When expressed in terms of the stopping number L, this approaches the expression

$$L^{(0)} = \ln B - \frac{1}{2} \tag{14}$$

at high speed. For $a=v/\omega$ we find

$$B = \frac{2mv^2}{\hbar\omega}, \tag{15}$$

i.e., Eq. (14) reduces to Bethe's stopping formula except for the term $-1/2$.

A similar observation can be made in classical stopping theory where, according to Bohr [4], the energy transfer $T(p)$ to a harmonic oscillator in distant collisions at an impact parameter p can be expressed as

$$T(p) = \frac{2Z_1^2e^4}{mv^2p^2}\left\{\left[\frac{\omega p}{v}K_1\left(\frac{\omega p}{v}\right)\right]^2 + \left[\frac{\omega p}{v}K_0\left(\frac{\omega p}{v}\right)\right]^2\right\}, \tag{16}$$

where K_0 and K_1 are modified Bessel functions in standard notation [22]. It has been shown [10] that binary scattering theory employing the Yukawa potential with $a=v/\omega$ reproduces the first term in the brackets. The missing part, i.e., the term containing K_0, can be integrated [Eq. (6.576.4) in Ref. [23]] and is seen to contribute a term $+1/2$ to the stopping number.

We may conclude that both in classical theory and in the first Born approximation, binary scattering theory with a Yukawa potential and a screening radius $a=v/\omega$ can replace bare-Coulomb scattering on a bound particle to a good approximation. The error amounts to a term in the stopping number which approaches a constant value $-1/2$ at high projectile speed, *both* in classical theory and Born approximation.

2. Phase shifts

Even though numerous studies have been performed on scattering off a Yukawa potential [24], we find it appropriate to show a few comparisons of phase shifts calculated by Eqs. (8) and (9) with exact results found by numerical evaluation of the radial Schrödinger equation. We emphasize that comparisons in this section are performed with a *velocity-independent* screening radius a.

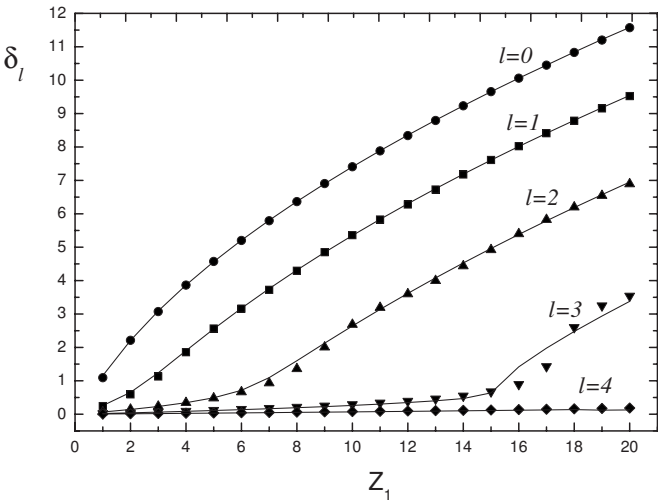

FIG. 1. Phase shifts for Yukawa potential with $k=1$ and $a=1$ in atomic units, $e=m=\hbar=1$. Symbols: Exact values from numerical integration of Eq. (7). Lines: Semiclassical, from Eq. (8).

Figure 1 shows calculated phase shifts for $k=1$ a.u., i.e., $v=v_0$, as a function of the atomic number Z_1 of the scattering center. Excellent agreement is found between semiclassical and exact results for $\ell=0$ and 1. Increasing discrepancies are observed for $\ell \geqslant 2$ as Z_1 increases.

Figure 2 shows similar data, but now for $k=5$ a.u. and as a function of ℓ. Excellent agreement is found here, also for those cases where discrepancies were evident for $k=1$ a.u. in Fig. 1.

The perturbative approximation (9) (not shown in the figures) yields significant discrepancies with increasing Z_1. However, the agreement improves with increasing k, i.e., at higher speed.

Figure 3 compares phase shifts for attractive and repulsive interaction, $Z_1=\pm 7$. Again, excellent agreement is found between exact results and semiclassical values of Eq. (8). The dotted line, which originates in Eq. (9), does not distinguish between positive and negative projectiles. With the exception of the range $0 \leqslant \ell \leqslant 2$, this approximation shows the ex-

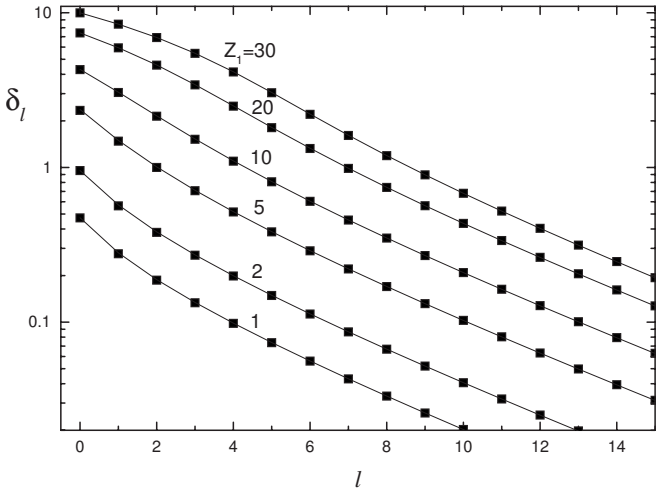

FIG. 2. Same as Fig. 1 for $k=5$ and $a=1$ a.u. with ℓ as the abscissa variable and an expanded parameter range.

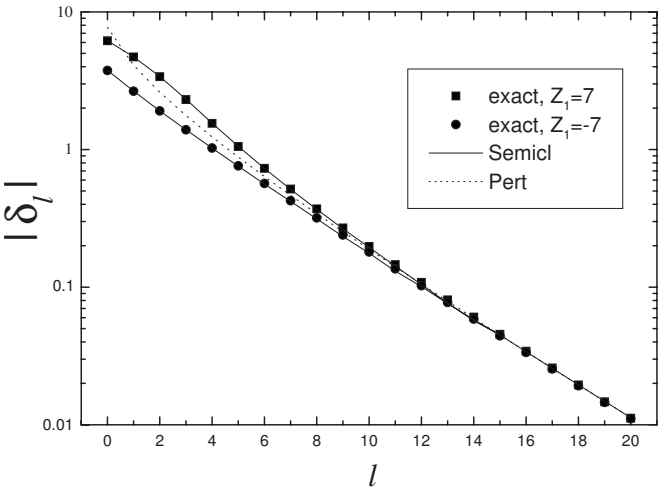

FIG. 3. Phase shifts for $Z_1=\pm 7$, $k=2$, and $a=2$ a.u. Solid lines: Eq. (8). Dotted line: Eq. (9).

pected behavior with phase shifts close to the average between the exact values for $Z_1=\pm 7$.

D. Analytic approximation

We find it desirable to have a convenient analytical approximation for the stopping cross section. We start by rewriting the transport cross section, Eq. (4), in the form

$$\sigma_{\rm tr}=\frac{4\pi}{k^2}\sum_{\ell=0}^{\infty}(\ell+1)\frac{\tan^2\Delta_\ell}{1+\tan^2\Delta_\ell}, \tag{17}$$

where

$$\Delta_\ell=\delta_\ell-\delta_{\ell+1}. \tag{18}$$

In the perturbative limit, where $\delta_\ell \ll 1$ and hence also $\Delta_\ell \ll 1$, this reduces to

$$\sigma_{\rm tr}^{\rm pert}=\frac{4\pi}{k^2}\sum_{\ell=0}^{\infty}(\ell+1)\Delta_\ell^2, \tag{19}$$

which is strictly quadratic in the perturbation when Δ_ℓ is approximated by Eq. (9). In the following this will be denoted as the perturbative limit.

The perturbative approximation is bound to break down for large phase shifts. Taylor expansion in powers of the interaction strength Z_1 is of little help in the case of strong coupling. Instead, we aim at an interpolation formula approaching the free-Coulomb limit but ignoring the Barkas-Andersen effect. The validity of the result will be verified by comparison with SCL1, and the main application area will be an extended Bloch correction for both bare and screened ions.

To this end we approximate Eq. (17) by

$$\sigma_{\rm tr}=\frac{4\pi}{k^2}\sum_{\ell=0}^{\infty}(\ell+1)\frac{\Delta_\ell^2}{1+\Delta_\ell^2}, \tag{20}$$

where we have kept the term Δ_ℓ^2 in the denominator. This expression reduces to Eq. (19) for small phase shifts, but unlike (19), the fraction $\Delta_\ell^2/(1+\Delta_\ell^2)$ never exceeds 1, as required by Eq. (4). As we will show by numerical examples, Eq. (20) is a suitable basis for analytical interpolations beyond the perturbative limit.

Now, for the Yukawa potential, Eq. (9) yields [25,26]

$$\delta_\ell^{\rm pert}=\eta K_0(x_\ell) \tag{21}$$

with

$$x_\ell=\frac{\ell+1/2}{ka}. \tag{22}$$

For large ℓ, we may approximate

$$\Delta_\ell=\eta[K_0(x_\ell)-K_0(x_{\ell+1})]\simeq\frac{\eta}{ka}K_1(x_\ell). \tag{23}$$

However, as we have seen in Fig. 3, the perturbative approximation does not describe phase shifts well for small ℓ. We have found that multiplication by $(\ell+1/2)/(\ell+1)$ allows one to repair this error [27]. Figure 4 shows that the expression

$$\Delta_\ell=\frac{\ell+1/2}{\ell+1}\frac{\eta}{ka}K_1(x_\ell)=\frac{\eta}{\ell+1}x_\ell K_1(x_\ell) \tag{24}$$

approaches Eq. (23) asymptotically for large ℓ and yields results very close to the exact phase-shift differences also for small ℓ, including the important case of $\ell=0$ where Eq. (23) fails drastically.

Now, consider specifically the case of unscreened Coulomb scattering, where $a=\infty$ and, hence, $x_\ell=0$. Then, Eq. (24) reduces to

$$\Delta_\ell=\frac{\eta}{\ell+1}, \tag{25}$$

and hence

$$\sigma_{\rm tr}=\frac{4\pi}{k^2}\eta^2\sum_{\ell=0}^{\infty}\frac{\ell+1}{(\ell+1)^2+\eta^2}, \tag{26}$$

which is the exact result for Coulomb scattering [28].

Approximating the transport cross section by Eq. (20), with Δ_ℓ defined by Eq. (23), i.e.,

$$\sigma_{\rm tr}^{SCL2}=\frac{4\pi}{k^2}\sum_{\ell}\frac{(\ell+1)[\eta x_\ell K_1(x_\ell)]^2}{(\ell+1)^2+[\eta x_\ell K_1(x_\ell)]^2} \tag{27}$$

will be referred to in the following as SCL2. We conclude that this approximation (i) is generally valid in the perturbation limit, (ii) approximates semiclassical phase shifts, averaging between positive and negative Z_1 for both small and large ℓ, and (iii) produces the exact (albeit divergent, as it has to be in the absence of screening and/or binding) transport cross section for straight Coulomb interaction.

Test results supporting the validity of the SCL2 approximation are shown in Fig. 5 as well as in Figs. 7 and 8 to be discussed later. Figure 5 shows transport cross sections for $Z_1=\pm 5$ and ± 20. From Fig. 4 we may extract that phase shifts become large in particular in the low-velocity range included in these graphs. Evidently, transport cross sections

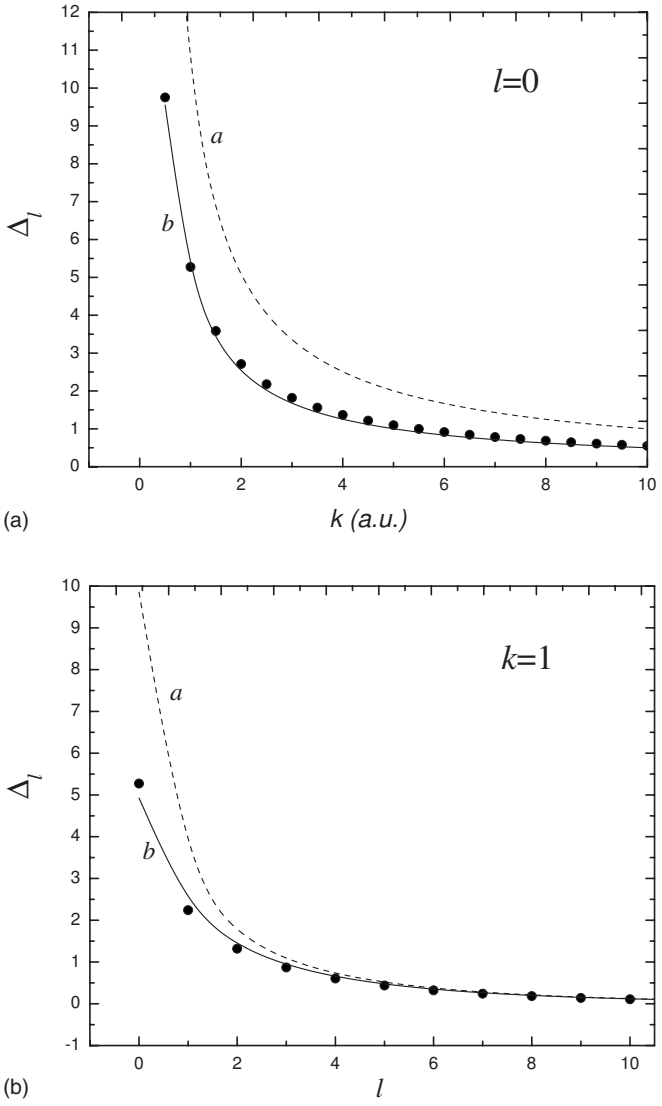

FIG. 4. Comparison of approximate phase-shift difference from Eq. (23) (curve *a*) and (24) (curve *b*) with exact values (solid circles), for $Z_1=5$ and $a=5$ a.u. Upper graph: k dependence for $\ell=0$. Lower graph: ℓ dependence for $k=1$ a.u.

are well represented by the semiclassical approximation SCL1, but also the SCL2 approximation delivers results intermediate between $Z_1=\pm 5$ over the entire velocity range.

III. STOPPING AT INTERMEDIATE VELOCITIES

A. Extended Bloch correction

Lindhard and Sørensen [28] defined a Bloch correction by the relation

$$\Delta\sigma_{\rm tr} = \sigma_{\rm tr} - \sigma_{\rm tr}^{\rm pert}, \tag{28}$$

where $\sigma_{\rm tr}$ was the exact transport cross section for free-Coulomb scattering and $\sigma_{\rm tr}^{\rm pert}$ its perturbative limit. We may generalize this relation for screened-Coulomb interaction, and we could describe the latter in terms of exact phase shifts as well as the SCL1 and the SCL2 approximation. Here we show results for the SCL2 and the SCL1 approximation.

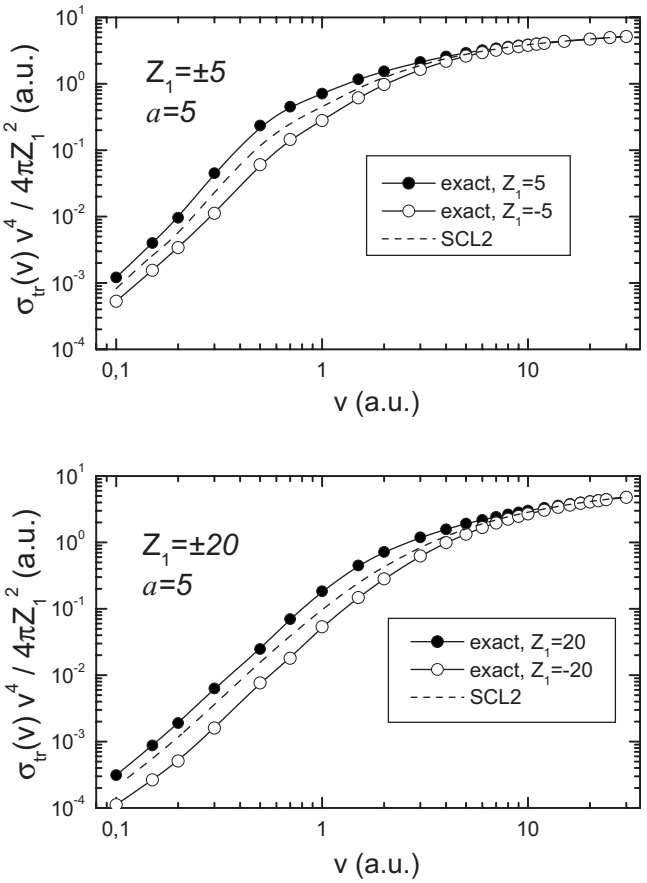

FIG. 5. Transport cross sections for Yukawa potential according to Eq. (4) (solid lines) with $a=5$ a.u. and $Z_1=\pm 5$ (upper graph) and $Z_1=\pm 20$ (lower graph). Points: Evaluated with exact phase-shift values from Eq. (7). Dashed line: Eq. (20).

For the SCL2 approximation we find the simple analytic expression

$$\Delta\sigma_{\rm tr} = \sigma_{\rm tr}^{\rm SCL2} - \sigma_{\rm tr}^{\rm pert} = -\frac{4\pi}{k^2}\sum_{\ell}(\ell+1)\frac{\Delta_\ell^4}{1+\Delta_\ell^2} \tag{29}$$

or, from Eq. (2), the equivalent stopping number,

$$\Delta L = -\frac{1}{\eta^2}\sum_{\ell}(\ell+1)\frac{\Delta_\ell^4}{1+\Delta_\ell^2}. \tag{30}$$

Insertion of Eq. (24) leads to

$$\Delta L = -\eta^2\sum_{\ell}\frac{[x_\ell K_1(x_\ell)]^4}{(\ell+1)\{(\ell+1)^2+[\eta x_\ell K_1(x_\ell)]^2\}}. \tag{31}$$

Figure 6 shows ΔL obtained from Eq. (31) as a function of the inverse Sommerfeld parameter $1/\eta = v/Z_1 v_0$. Here we have set $a=v/\omega$ in accordance with Eq. (11). The term for $\ell=0$ dominates the sum, and terms with $\ell \geqslant 2$ contribute altogether a few percent. This is consistent with the view of the Bloch correction as being related to close collisions [14]. We remind that ℓ/k is a quantum analog of the classical impact parameter.

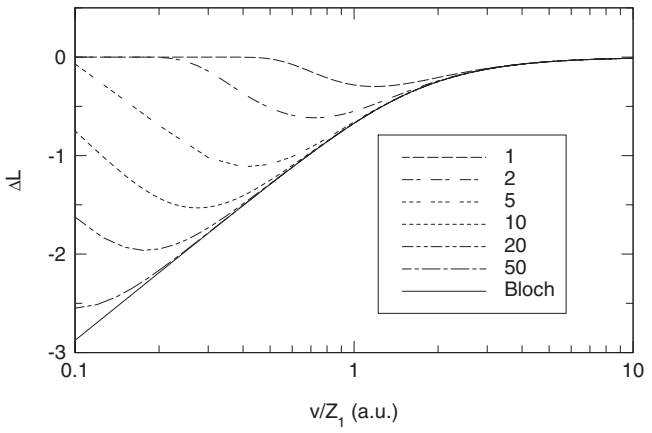

FIG. 6. Extended Bloch correction according to Eq. (31) for $a=v/\omega$ and $\omega=1$ a.u. Labels indicate the atomic number Z_1 of the projectile. Solid line: Eq. (32).

In addition to the results for a variety of Z_1 values, we have also included the standard Bloch correction which follows from Eq. (26) according to Ref. [28] and reads

$$\Delta L_{\mathrm{Bloch}} = \mathrm{Re}[\psi(1) - \psi(1 + i\eta)] \tag{32}$$

in conventional notation, where $\psi(x)$ is the digamma function [22]. It is seen that all curves merge into the Bloch curve at high speed, but at low projectile speed, where the Bloch correction shows a logarithmic divergence, the present estimate exhibits a more adequate behavior.

A more detailed analysis of this behavior using the SCL1 approximation is shown in Fig. 7. Here, for the SCL1 approximation the Bloch correction has been evaluated on the basis of the more accurate phase shifts obtained from Eq. (8). Figure 7 shows results for positive and negative Z_1 together with the corresponding results from SCL2. It is seen that the latter is very close to the average between the two former, represented by dashed lines.

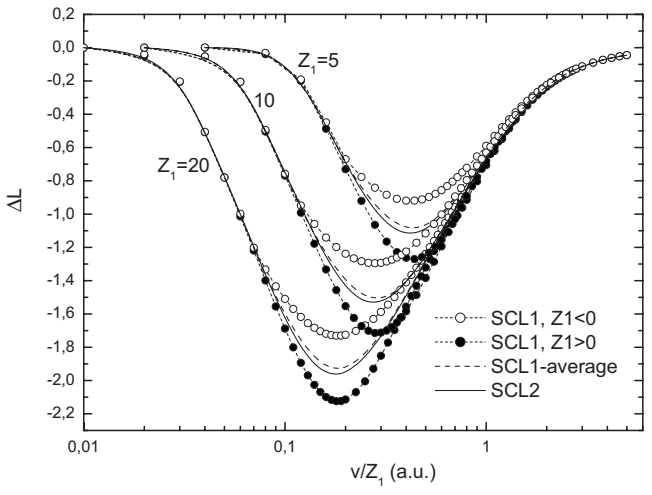

FIG. 7. Generalized Bloch correction evaluated from SCL1 (symbols) and SCL2 (solid lines) approximation for $Z_1=\pm 5$, 10, 20. Dashed lines indicate the average between positive and negative Z_1.

B. The missing term in the stopping number

It was mentioned in Sec. II C 1 that modeling the stopping cross section as a binary-scattering problem on a screened-Coulomb potential misses a term approaching $\frac{1}{2}$ in the stopping number at high speed. In classical binary stopping theory [10], this term was interpreted as a potential-energy transfer and evaluated as

$$W = \frac{1}{2} m\omega^2 r_{\mathrm{eff}}^2, \tag{33}$$

where the effective distance r_{eff} is governed by the angular-momentum transfer. Even though there is no potential-energy transfer in free binary scattering, there is transfer of angular momentum around the initial location of the target electron. For a classical scattering event at an impact parameter p, this leads to the relation [10]

$$r_{\mathrm{eff}} = 2\tau - p\theta, \tag{34}$$

where

$$\tau = \sqrt{r_m^2 - p^2} - \int_{r_m}^{\infty} dr \left(\frac{1}{\sqrt{1 - V(r)/E_r - p^2/r^2}} - \frac{1}{\sqrt{1 - p^2/r^2}} \right) \tag{35}$$

is the time integral and

$$\theta = \pi - 2p \int_{r_m}^{\infty} \frac{dr}{r^2} \left(1 - \frac{V(r)}{E_r} - \frac{p^2}{r^2} \right)^{-1/2} \tag{36}$$

the center-of-mass system scattering angle [3]. Here, r_m is a root of the relation $1-V(r)/E_r-p^2/r^2=0$ and p the impact parameter.

We may arrive at a quantum analog of this expression by making the replacements

$$v = \frac{\hbar k}{m} \quad \text{and} \quad p = \frac{\ell + 1/2}{k}, \tag{37}$$

with the result

$$r_{\mathrm{eff}} = -\frac{2}{k} \left(\delta_\ell + \int dr \frac{2mV(r)/\hbar^2}{\sqrt{k^2 - 2mV(r)/\hbar^2 - (\ell + 1/2)^2/k^2}} \right). \tag{38}$$

In the perturbation limit, Eq. (38) reduces to

$$r_{\mathrm{eff}} = \frac{2Z_1 e^2}{mv^2} K_0\left(\frac{\omega p}{v} \right) = \frac{2Z_1 e^2}{mv^2} K_0\left(\frac{2\ell + 1}{B} \right), \tag{39}$$

where B is defined by Eq. (15). With this, Eq. (33) produces the second term in Eq. (16).

In the spirit of the semiclassical picture we replace the integration over the impact parameter by a summation over ℓ so that

$$\int_0^{\infty} 2\pi p dp W(p) \to 2\pi \left(\frac{\hbar}{mv} \right)^2 \sum_{\ell=0}^{\infty} (\ell + 1/2) W(\ell). \tag{40}$$

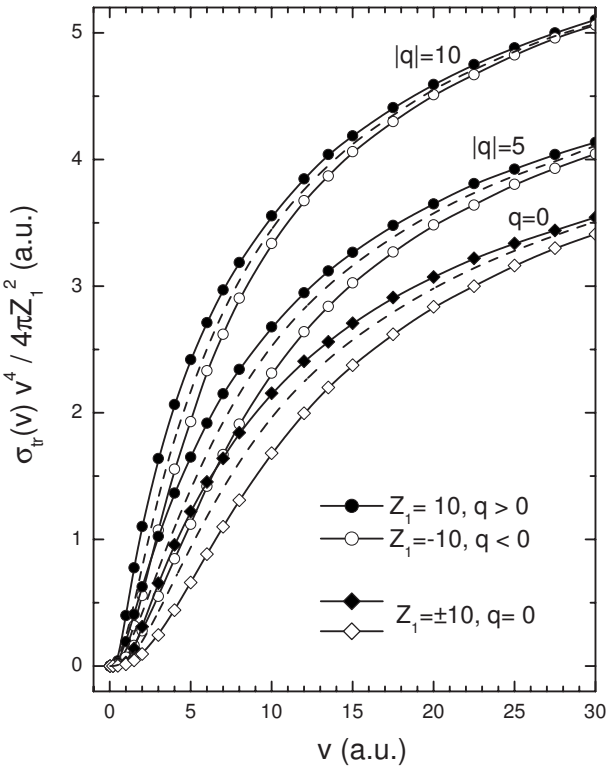

FIG. 8. Transport cross section for dressed ion with $Z_1=\pm 10$, $a_1=1$, $a_2=5$ a.u. and three different charge states $q=\pm 10, \pm 5, 0$. Notation as in Fig. 5.

C. Dressed ions

The analysis presented so far applies to a bare ion, where screening simulates the effect of binding. We now generalize the description to ions carrying electrons. We consider here a model where the interaction with the target electrons is described by a two-component potential,

$$V(r) = -\frac{q_1 e^2}{r} e^{-r/a_1} - \frac{q_2 e^2}{r} e^{-r/a_2}, \tag{41}$$

with $q_1+q_2=Z_1$ and two screening radii a_1, a_2. Equation (41) reflects the internal screening due to localized core electrons on the projectile and external screening discussed in the previous paragraphs. The model used in Refs. [10,29] belongs in this category.

Within the SCL2 scheme, the approximations made through Eqs. (20)–(24) may be repeated with the present ion model. Instead of Eq. (24), Δ_ℓ in Eq. (20) now reads

$$\Delta_\ell = \frac{\eta}{\ell+1}\left[\frac{q_1}{Z_1} x_\ell^{(1)} K_1(x_\ell^{(1)}) + \frac{q_2}{Z_1} x_\ell^{(2)} K_1(x_\ell^{(2)})\right], \tag{42}$$

where

$$x_\ell^{(1)} = \frac{\ell+1/2}{k a_1}; \quad x_\ell^{(2)} = \frac{\ell+1/2}{k a_2}. \tag{43}$$

Figure 8 shows transport cross sections for ions with atomic numbers $Z_1=\pm 10$ for charge states $q\equiv q_2=0$, 5, and 10. To illustrate the magnitudes of the Barkas-Andersen and Bloch corrections we have also included curves for "image ions" with $Z_1<0$, representing an antinucleus surrounded by a cloud of positrons, even though their practical significance is fairly remote in the present context. As in previous examples, the full semiclassical approximation, Eq. (8), reproduces the exact results very well, and the SCL2 approximation using Eq. (42) describes approximately the average behavior.

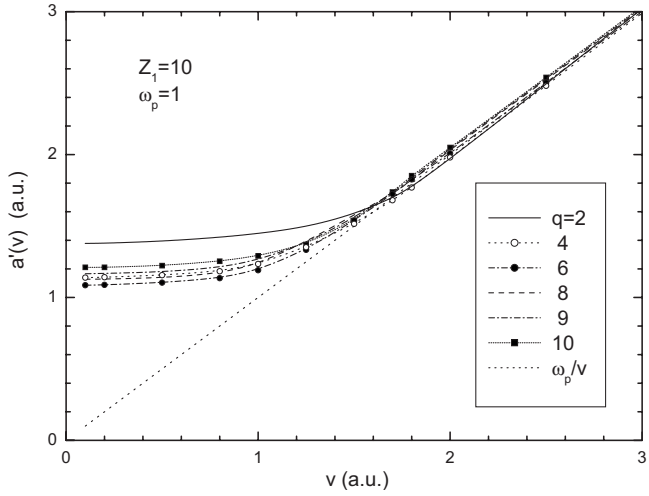

FIG. 9. Dynamic-screening radius a' determined from the generalized Friedel sum rule. See text.

Evidently, the particle-antiparticle difference is greatest for the neutral projectile, where the potential deviates most pronouncedly from bare-Coulomb interaction.

In order to generate an extension of the Bloch correction to ions carrying bound electrons, we need specific values for the screening radii. Here we have adopted the expressions

$$a_1 = \left(\frac{1}{a_{\rm sc}^2} + \frac{1}{a'^2}\right)^{-1/2}, \tag{44}$$

$$a_2 = a', \tag{45}$$

where $a_{\rm sc}=(1-q_1/Z_1)a_{\rm TF}$ is the charge-dependent static-screening radius [29], $a_{\rm TF}=0.8853a_0/Z_1^{1/3}$ the Thomas-Fermi radius of a neutral projectile, and a' a dynamic-screening radius which, for the special case of the Fermi gas, can be determined by requiring the generalized Friedel sum rule [30] to be fulfilled. For $a'=v/\omega$, Eq. (45) reduces to the set of screening radii adopted in Ref. [10], which has been shown to deliver the exact asymptotic behavior of the kinetic-energy transfer at high projectile speed and large impact parameters. The present generalization extends the range of validity to low velocities.

Figure 9 shows that $a'(v)$ is rather insensitive to the charge state. This is an essential feature in the present context. We emphasize that the rapid approach to the asymptotic behavior, $a'=v/\omega_P$, is not a postulate but results from application of the generalized Friedel rule.

Figure 10 shows extended-Bloch corrections $\Delta L=L-L^{\rm pert}$ for $Z_1=10$ and charge states ranging from 0 to Z_1, evaluated in the SCL2 approximation. The magnitude of the correction is found to decrease significantly with the charge

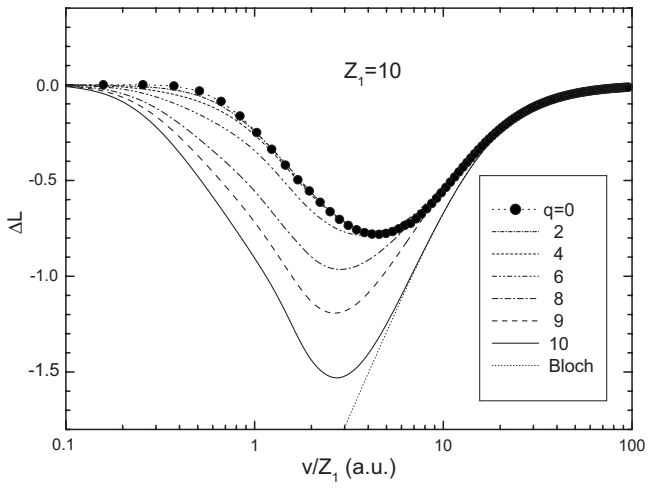

FIG. 10. Extended Bloch correction ΔL for dressed ion, evaluated in the SCL2 approximation for $Z_1=10$ and charge states 0, 2, 4, 6, 8, and 10 for $\omega=1$ a.u. The scattering potential is defined by Eqs. (41) and (45). The dotted line shows the standard Bloch correction Eq. (32) for bare ions.

state from $q=10$ to 6, whereafter it is found to remain nearly constant [31].

In order to ensure that the behavior shown in Fig. 10 is not just an artifact of our choice of screening parameters, we also performed an equivalent calculation with the simpler choice $a_1=a'$. As expected, this gave rise to different values of a' but very similar results for the generalized Bloch correction.

D. Allowance for orbital motion

The discussion up to this point refers to target electrons at rest. When electrons move with an orbital velocity $\vec{v}_e$, determination of the stopping cross section requires a change of reference frame. For binary collisions the pertinent generalization of Eq. (2) has been derived in Ref. [32],

$$S(v) = \left\langle m\vec{v}\cdot\vec{v}_r\frac{v_r}{v}\sigma_{\mathrm{tr}}(v,v_r)\right\rangle_{\vec{v}_e}, \tag{46}$$

where $\vec{v}_r=\vec{v}-\vec{v}_e$ is the relative velocity, the average is taken over the distribution of orbital velocities, and the reduction to a readily managable double integral has been described in Refs. [26,33].

For a fixed potential, the transport cross section in Eq. (46) depends only on the relative speed $v_r=|\vec{v}-\vec{v}_e|$. However, both the adiabatic radius $a_{\mathrm{ad}}=v/\omega$ and the equilibrium charge state depend on the laboratory speed v. This has been expressed by the dependence on two variables of the transport cross section.

Figure 11 shows stopping cross sections for protons in a free-electron gas, obtained from Eq. (46) for $\omega_P=0.5$ a.u. Semiclassical approximations and the perturbation limit are shown, together with a generalized Bloch correction, again defined as the difference between the curve labeled SCL2 and its perturbative limit. Also included is the result of Ref. [34], Lindhard and Winther (LW), which represents the Born

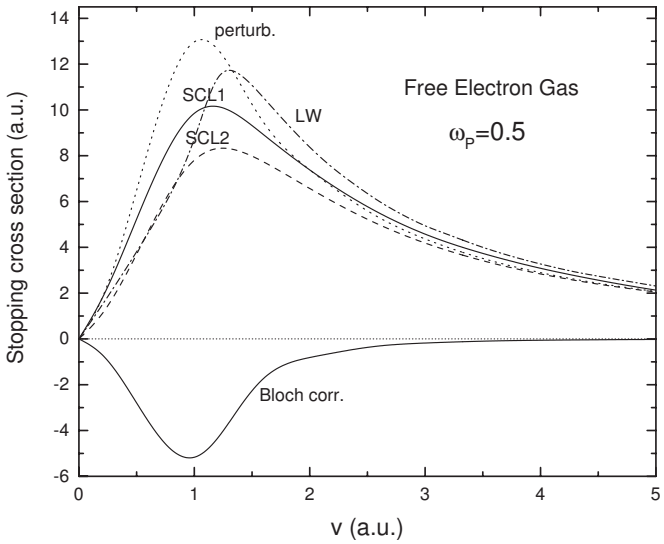

FIG. 11. Stopping cross section per target electron for protons in a Fermi gas with a plasma frequency $\omega_P=0.5$ a.u. obtained from Eq. (46). Solid line: Based on Eq. (8). Dashed line: Based on Eq. (20). Dotted line: Based on Eq. (19). Dotted-dashed line: From [34]. The generalized Bloch correction is the difference between the dashed and the dotted line.

approximation for the electron gas. The difference between SCL1 and SCL2 represents the Barkas-Andersen effect, while the difference between LW and SCL1 for $v\gg v_0$ reflects the missing term mentioned in Sec. III B. At velocities $v\lesssim v_0$, the SCL1 approximation must be superior to the Born approximation.

Similar comments apply to Fig. 12 which shows the corresponding graph for a target electron bound harmonically. Here, the Born approximation is represented by the result from Ref. [35] [Sigmund and Haagerup (SH)].

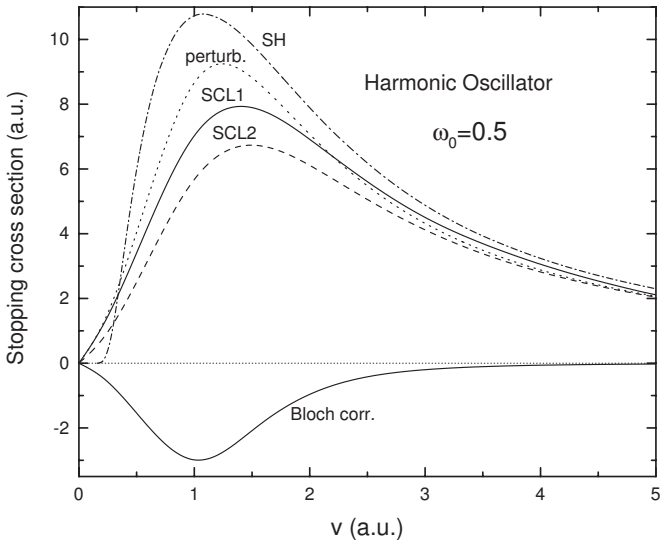

FIG. 12. Same as Fig. 11 for harmonic oscillator with a resonance frequency $\omega=0.5$ a.u. The dotted-dashed curve reflects the Born approximation from Ref. [35].

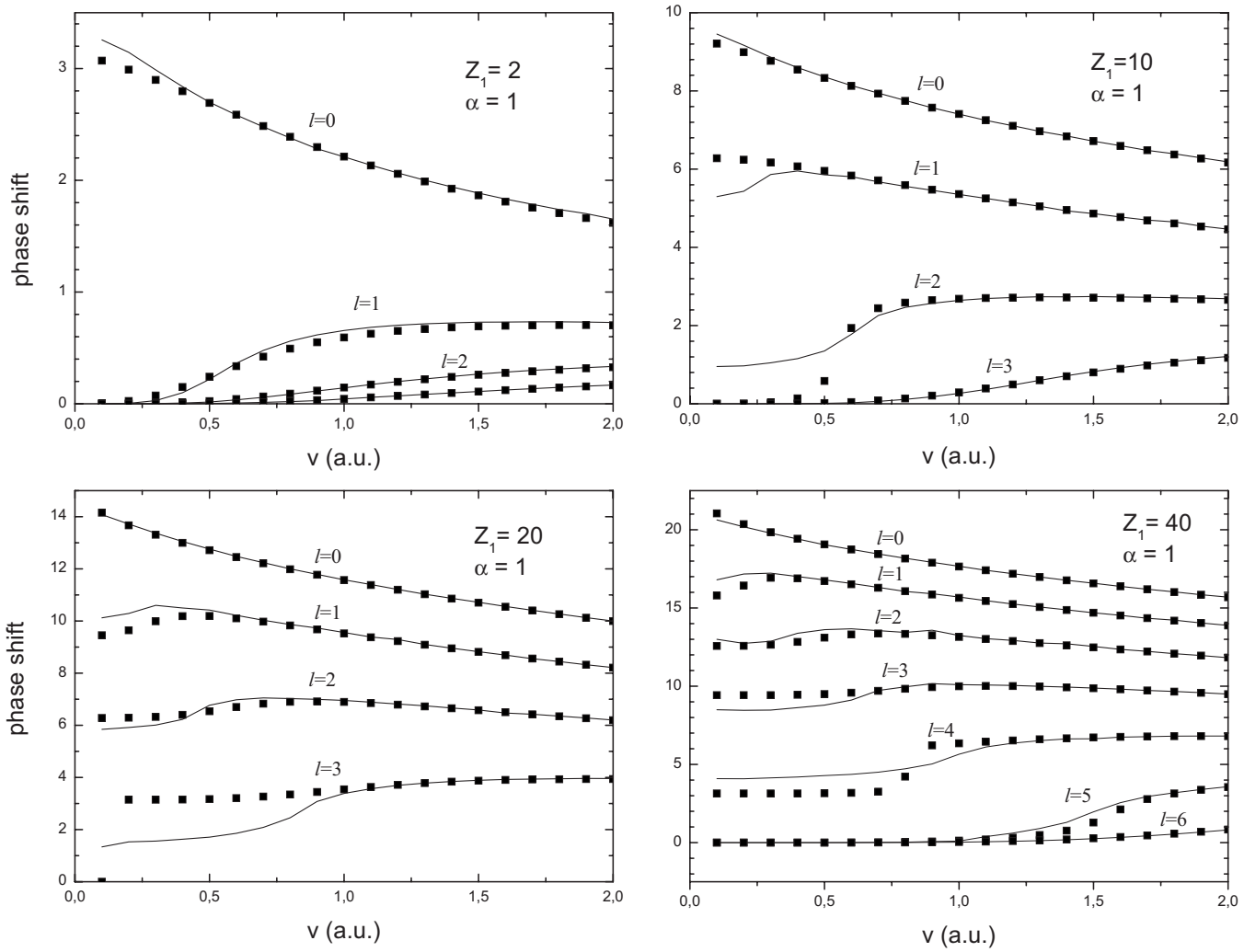

FIG. 13. Phase shifts for Yukawa potential with $a=1$ a.u. Points: Exact, from Eq. (7). Lines: Semiclassical results from Eq. (8).

IV. STOPPING AT LOW VELOCITIES

A. Introductory remarks

At low projectile speed one may expect a fundamental difference between excitation of free and bound electrons. Indeed, it is well known that excitation of bound electrons by slow heavy ions is, to some extent, influenced by electron promotion, a process very different from Coulomb excitation. This is not the case for a free-electron gas: While the plasma frequency takes the place of the binding frequency in the interaction with high-speed projectiles, it loses relevance at low speed, where the Fermi speed becomes the important parameter [34].

Numerous calculations have been performed for stopping in a Fermi gas, which may serve as a standard of comparison [7,11,18,26,30,34,36–39]. Therefore, the following discussion will be limited to the Fermi gas.

B. Phase shifts

At low projectile speed the transport cross section is governed by contributions from small values of ℓ. Therefore, a more detailed test is indicated before application of the scheme to low-velocity stopping.

Figure 13 shows comparisons of the type shown previously, but now specifically for the low-velocity range $v \leqslant 2v_0$ for $\ell=0$ to 6 and $Z_1=2$, 10, 20, and 40. Systematic discrepancies are observed at the lowest velocities, in particular for $\ell=1$ to 4, while the dominating phase shift for $\ell=0$ appears to be well described by the semiclassical scheme. Note, however, that according to Eq. (47) below, errors in the phase shifts at projectile speeds below the Fermi velocity are immaterial in the present context.

C. Transport cross section

Figure 14 illustrates the general behavior of the transport cross section [40] as a function of v_r for Yukawa interaction with a fixed screening parameter $a=a_0$. The range of relative velocities includes common Fermi velocities in metals. A pronounced oscillatory behavior is found for $v_r/v_0=1$ and 0.5, which is strongly damped and has essentially disappeared for $v_r/v_0=2$. This behavior is well established [11,36–38]. At this point we just note that the agreement

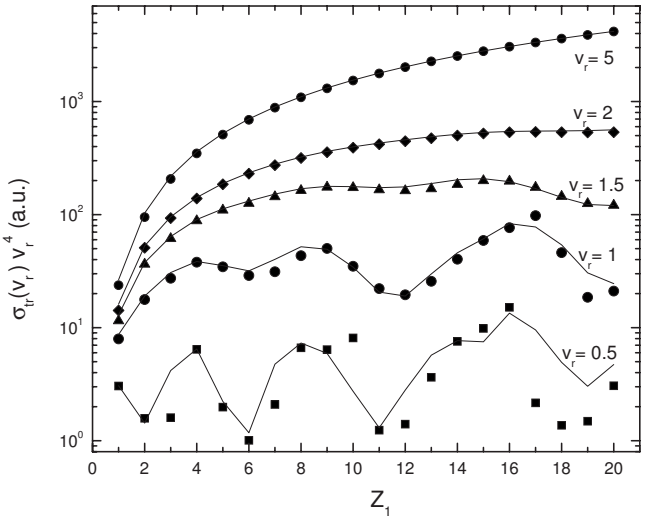

FIG. 14. Transport cross section $\sigma_{tr}(v_r)$ versus Z_1 evaluated from Eq. (4). Points: Exact phase shifts from Eq. (7). Lines: Semiclassical phase shifts from Eq. (8). Yukawa potential with fixed $a=1$ a.u., $r_s=1.6$, or $v_F=1.2$.

between the semiclassical approximation and the exact phase shifts for the given potential is good for $v_r/v_0=1$. For $v_r/v_0=0.5$ significant differences show up, but at least the qualitative behavior is still reproduced.

D. Z_1 structure: Application of Friedel sum rule

At beam velocities small compared to the Fermi speed, $v \ll v_F$, the stopping cross section per target electron reduces to [41]

$$S = mvv_F\sigma_{tr}(v_F). \tag{47}$$

For a more quantitative picture we need a more reliable potential function. To this end we have studied two trial functions containing an adjustable parameter which, following a procedure proposed in Ref. [39], has been chosen such as to satisfy the Friedel sum rule [42,43]

$$\frac{2}{\pi}\sum_{\ell=0}^{\infty}(2\ell+1)\delta_\ell^{\mathrm{SCL1}}(v_F) = Z_1. \tag{48}$$

In addition to the Yukawa potential with a free screening parameter a [44] we also studied the potential of a hydrogenlike atom,

$$V(r) = -Z_1e^2\left(\frac{1}{2a}+\frac{1}{r}\right)e^{-r/a}. \tag{49}$$

Phase shifts are calculated here from the semiclassical expression (8). After the values of a were determined by adjustment according to Eq. (48), the transport cross section was calculated from Eq. (4). The results of this approach were finally compared with those of *ab initio* calculations provided by the density functional theory (DFT) [45]. Figure 15 shows results for two typical values of the electron density representative for metals. We note that qualitative features are well represented. This appears gratifying in view of the simplicity of the present approach.

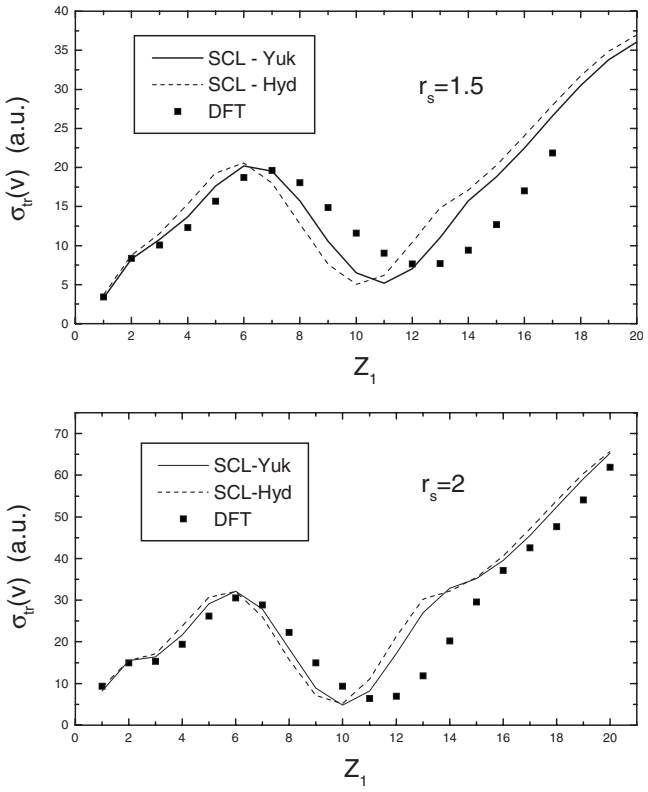

FIG. 15. Transport cross section at $v=v_F$ versus atomic number Z_1. Points: Based on density functional theory [45]. Lines: Phase shifts from semiclassical theory, Eq. (8), screening radius determined from Friedel sum rule. Solid line: Yukawa potential. Dotted line: Hydrogenic potential. Upper graph: $r_s=1.5$. Lower graph: $r_s=2$.

V. CONCLUSIONS

The semiclassical (SCL1) approach to stopping theory presented in this work has the benefit of incorporating the Bloch correction as well as the Barkas-Andersen effect from the beginning. Moreover, it reproduces Z_1 structure when applied to the Fermi gas at low projectile speed. A simplified version (SCL2), which is largely analytical, neglects the Barkas-Andersen effect but incorporates a Bloch correction in a form that is also applicable in the velocity range where static screening is important and Bloch's original expression shows a divergence. Although the SCL1 scheme is essentially numerical, computational requirements are very modest in comparison to existing quantal approaches. A weak point, which evidently needs more work, is the treatment of the potential-energy term which has been determined by analogy with classical stopping theory.

Apart from computational ease there are noticeable differences to alternative schemes:

(i) Binary stopping theory [10,17], based on classical scattering theory and a superimposed Bloch correction, ignores Z_1 structure.

(ii) The unitary-convolution approximation [12,46] neglects the Barkas-Andersen effect.

(iii) The HISTOP code [18] in its present form only allows application to the Fermi gas.

(iv) The close-coupling scheme of Refs. [47,48] is computationally very intensive.

(v) The convergent kinetic theory (CKT) scheme of Ref. [13], powerful but also complex, is geared primarily toward dense hot plasmas.

Applications discussed here mainly served the purpose of determining the accuracy and limitations of the approach. Applications to specific ion-target systems have been reserved to furthcoming work.

ACKNOWLEDGMENTS

Part of this work has been performed during several mutual visits. The work of one of us (N.R.A.) was supported by a grant from the Carlsberg Foundation. Support from the ANPCYT of Argentina (Contract No. PICT R-122/02) and from the Danish Natural Science Research Council (FNU) is gratefully acknowledged.

[1] N. Bohr, Mat. Fys. Medd. K. Dan. Vidensk. Selsk. **18** (8), 1 (1948).
[2] M. A. Kumakhov and F. F. Komarov, *Energy Loss and Ion Ranges in Solids* (Gordon and Breach, New York, 1981).
[3] P. Sigmund, *Particle Penetration and Radiation Effects*, Springer Series in Solid-State Sciences No. 151 (Springer, Berlin, 2006).
[4] N. Bohr, Philos. Mag. **25**, 10 (1913).
[5] H. Bethe, Ann. Phys. **5**, 324 (1930).
[6] F. Bloch, Ann. Phys. **16**, 285 (1933).
[7] P. M. Echenique, F. Flores, and R. H. Ritchie, Solid State Phys. **43**, 229 (1990).
[8] P. Sigmund, *Stopping of Heavy Ions*, Springer Tracts of Modern Physics No. 204 (Springer, Berlin, 2004).
[9] *Stopping of Heavy Ions—STOP 01*, edited by H. H. Andersen and P. Sigmund, special issue of Nucl. Instrum. Methods Phys. Res. B 195 (2002).
[10] P. Sigmund and A. Schinner, Eur. Phys. J. D **12**, 425 (2000).
[11] N. R. Arista, Nucl. Instrum. Methods Phys. Res. B **195**, 91 (2002).
[12] P. L. Grande and G. Schiwietz, Nucl. Instrum. Methods Phys. Res. B **195**, 55 (2002).
[13] G. Maynard, C. Deutsch, K. Dimitriou, K. Katsonis, and M. Sarrazin, Nucl. Instrum. Methods Phys. Res. B **195**, 188 (2002).
[14] A. H. Sørensen, Phys. Rev. A **55**, 2896 (1997).
[15] V. A. Khodyrev, J. Phys. B **33**, 5045 (2000).
[16] A. Bohr, Mat. Fys. Medd. K. Dan. Vidensk. Selsk. **24**(19), 1 (1948).
[17] P. Sigmund and A. Schinner, Nucl. Instrum. Methods Phys. Res. B **195**, 64 (2002).
[18] N. R. Arista and A. F. Lifschitz, Adv. Quantum Chem. **45**, 47 (2004).
[19] N. F. Mott and H. S. W. Massey, *The Theory of Atomic Collisions* (Oxford University Press, London, 1949).
[20] L. D. Landau and E. M. Lifshitz, *Quantum Mechanics. Non-Relativistic Theory*, Course of Theoretical Physics No. 3 (Pergamon Press, Oxford, 1960).
[21] J. Lindhard, Nucl. Instrum. Methods **132**, 1 (1976).
[22] M. Abramowitz and I. A. Stegun, *Handbook of Mathematical Functions* (Dover, New York, 1964).
[23] I. S. Gradshteyn and I. M. Ryzhik, *Table of Integrals, Series, and Products*, 5th ed. (Academic Press, San Diego, 1980).
[24] C. J. Joachain, *Quantum Collision Theory* (North-Holland, Amsterdam, 1983).
[25] J. A. Brinkman, J. Appl. Phys. **25**, 961 (1954).
[26] L. de Ferrariis and N. R. Arista, Phys. Rev. A **29**, 2145 (1984).
[27] We remind that replacement of $\ell(\ell+1)$ by $(\ell+1/2)^2$ is a standard step in semiclassical quantum theory [20].
[28] J. Lindhard and A. H. Sørensen, Phys. Rev. A **53**, 2443 (1996).
[29] P. Sigmund, Phys. Rev. A **56**, 3781 (1997).
[30] A. F. Lifschitz and N. R. Arista, Phys. Rev. A **57**, 200 (1998).
[31] Because of convergence problems in an attempt to determine $a'(v)$ for $q=0$ from the generalized Friedel sum rule, we made the choice $a'=a_{\mathrm{TF}}$ in this special case. This delivered a generalized-Friedel sum 10.3 instead of 10.0. However, Fig. 10 shows that the Bloch correction is insensitive to the charge state for q approaching zero.
[32] B. A. Trubnikov and Y. N. Yavlinskii, Zh. Eksp. Teor. Fiz. **48**, 253 (1965) [Sov. Phys. JETP **21**, 167 (1965)].
[33] P. Sigmund, Phys. Rev. A **26**, 2497 (1982).
[34] J. Lindhard and A. Winther, Mat. Fys. Medd. K. Dan. Vidensk. Selsk. **34** (4), 1 (1964).
[35] P. Sigmund and U. Haagerup, Phys. Rev. A **34**, 892 (1986).
[36] J. Finnemann, Master's thesis, Aarhus University, 1968.
[37] J. Briggs and A. Pathak, J. Phys. C **6**, L153 (1973).
[38] J. S. Briggs and A. P. Pathak, J. Phys. C **7**, 1929 (1974).
[39] T. L. Ferrell and R. H. Ritchie, Phys. Rev. B **16**, 115 (1977).
[40] The quantity $v_r^4\sigma_{\mathrm{tr}}$ has been plotted here in order to achieve a reader-friendly separation of the curves.
[41] Equation (47) appears to date back to unpublished work by Lindhard. A derivation from Eq. (46) may be found in Ref. [33], Eq. (81).
[42] J. Friedel, Philos. Mag. **43**, 153 (1952).
[43] J. Friedel, Adv. Phys. **3**, 446 (1954).
[44] We have assumed here that the ion is neutral, i.e., $q_2=0$. Therefore, direct determination of a here is equivalent with determining a' in Eq. (45).
[45] M. J. Puska and R. M. Nieminen, Phys. Rev. B **27**, 6121 (1983).
[46] P. L. Grande and G. Schiwietz, CasP version 3.1 (2004), URL www.hmi.de/people/schiwietz/casp.html
[47] P. L. Grande and G. Schiwietz, Phys. Rev. A **44**, 2984 (1991).
[48] G. M. Azevedo, P. L. Grande, and G. Schiwietz, Nucl. Instrum. Methods Phys. Res. B **164-165**, 203 (2000).